

# NAVIER-STOKES COMPUTATIONS ON FLEXIBLE ADVANCED TRANSPORT-TYPE WING CONFIGURATIONS IN TRANSONIC REGIME

Guru P. Guruswamy \* and Eugene L. Tu\*\*

Computational Aerosciences Branch

NASA Ames Research Center, Moffett Field, California 94035-1000

## Abstract

Steady, unsteady and aeroelastic computations are performed on advanced transonic wing and wing-body configurations. The flow is modeled by the Navier-Stokes equations and structures for aeroelastic computations are modeled by the modal equations. The inadequacy of Euler equations and importance of using the Navier-Stokes equations with turbulence model is demonstrated for supercritical flows in the transonic regime. Effect of Mach number on steady pressure distributions are illustrated. Steady flow computations for transonic wings are compared with wind tunnel data and also with equivalent conventional wings. Unsteady computations are made in the context of demonstrating the use of the indicial approach for generating aerodynamic data for aeroelastic computations. By using the unsteady data generated by indicial responses, a computationally efficient approach of computing preliminary flutter boundaries is demonstrated. Effect of Mach number on the flutter boundary including the prediction of the 'transonic flutter speed dip' is demonstrated. The flutter boundaries of transonic wings are compared with equivalent conventional wings. Characteristics of the flutter boundaries are correlated with aerodynamic flow characteristics.

## Introduction

There is a continuous effort to improve the performance of subsonic transport aircraft.<sup>1</sup> One attempt is to improve the fuel efficiency by extending the flight regime to high sub-transonic Mach numbers to increase lift-to-drag ratios and flight speeds. To avoid the high drag associated with strong shock-waves, these advanced transports require modern wing sections such as supercritical wings that delay the shock-wave formation. Early experiments have shown that these advanced wings experience an undesirable reduction in

the flutter speed at the transonic regime. Such a phenomenon commonly known as 'transonic-dip', is more pronounced for wings with supercritical airfoils.<sup>2</sup> In order to accurately predict the flutter characteristics, it is necessary to model viscous flows using the Navier-Stokes equations.

To date, advanced wing calculations have been restricted to steady and unsteady computations on rigid wings. However, it is necessary to account for the wing's flexibility to accurately compute its aeroelastic characteristics. The aeroelastic deformation resulting from this flexibility can significantly change the nature of the flow. Strong interactions between the flow and structures can lead to sustained aeroelastic oscillations for swept wings.<sup>3</sup> Also, it is necessary to include the flexibility for proper correlations of computed data with experiments, particularly with those obtained from flight tests. To compute the flows accurately, it is necessary to include both aerodynamic and structural effects of the body. Recent efforts have been made to include the flexibility effects for wing-body configurations.<sup>4</sup> In this work, the flow is modeled using the Navier-Stokes equations and aeroelastic computations are made by using an uncoupled approach.

The computer code, ENSAERO computes the unsteady aerodynamics and aeroelasticity of aircraft by using the Thin Layer Navier-Stokes equations.<sup>5</sup> Previous work has demonstrated the code's capability to compute aeroelastic responses by simultaneously integrating the Navier-Stokes equations and the structural equations of motion, by using aeroelastically adaptive dynamic grids.<sup>4</sup> The flow is solved by time-accurate, finite-difference schemes based on the Beam-Warming algorithm with the Baldwin-Lomax turbulence model.

This work studies transonic aeroelastic characteristics of advanced transports. The LANN (Lockheed-Air Force-NASA-NLR) wing model<sup>6</sup> and Boeing 7J7<sup>1</sup> wing-body model are considered for this study. For both models the computed steady data are validated with the wind tunnel data. For the LANN model, steady flows are compared with models having equivalent conventional airfoil sections. For the LANN model, detailed aeroelastic computations are made to predict the 'transonic dip' and results are compared with the equivalent conventional wing. The characteristics of the flutter boundary are related to the aerodynamic flow characteristics. Preliminary flow characteristics that can be used for detailed aeroelastic analyses is studied

\* Research Scientist, AIAA Associate Fellow

\*\* Research Scientist, AIAA Member

Copyright © 1994 by the American Institute of Aeronautics and Astronautics, Inc. No copyright is asserted in the United States under Title 17, U.S. Code. The U.S. Government has a royalty-free license to exercise all rights under the copyright claimed herein for Governmental purposes. All other rights are reserved by the copyright owner.

for the Boeing 7J7 wing-body model.

### Governing Aerodynamic Equations

The strong conservation-law form of the Thin-Layer Navier-Stokes equations are used for shock capturing purposes. The thin-layer version of the equations in generalized coordinates can be written as<sup>7</sup>

$$\partial_\tau \hat{Q} + \partial_\xi \hat{E} + \partial_\eta \hat{F} + \partial_\zeta \hat{G} = Re^{-1} \partial_\zeta \hat{S} \quad (1)$$

where  $\hat{Q}$ ,  $\hat{E}$ ,  $\hat{F}$ ,  $\hat{G}$ , and  $\hat{S}$ , are flux vectors in generalized coordinates. The following transformations are used in deriving Eq. (1).

$$\begin{aligned} \tau &= t \\ \xi &= \xi(x, y, z, t) \\ \eta &= \eta(x, y, z, t) \\ \zeta &= \zeta(x, y, z, t) \end{aligned}$$

It should be emphasized that the thin-layer approximation is valid only for high Reynolds number flows and very large turbulent eddy viscosities invalidate the model.

To solve Eq. (1), ENSAERO has time-accurate methods based on both central-difference<sup>8</sup> and upwind schemes.<sup>9</sup> In this work the diagonal form of the Beam-Warming central difference scheme is used.

### Aeroelastic Equations of Motion

The governing aeroelastic equations of motion are obtained by using the Rayleigh-Ritz method. In this method, the resulting aeroelastic displacements at any time are expressed as a function of a finite set of assumed modes. The contribution of each assumed mode to the total motion is derived by the Lagrange's equation. Furthermore, it is assumed that the deformation of the continuous wing structure can be represented by deflections at a set of discrete points. This assumption facilitates the use of discrete structural data, such as the modal vector, the modal stiffness matrix, and the modal mass matrix. These can be generated from a finite-element analysis or from experimental influence coefficient measurements. In this study, the finite-element method is employed to obtain the modal data.

It is assumed that the deformed shape of the wing can be represented by a set of discrete displacements at selected nodes. From the modal analysis, the displacement vector  $\{d\}$  can be expressed as

$$\{d\} = [\phi]\{q\} \quad (2)$$

where  $[\phi]$  is modal matrix.

The final matrix form of the aeroelastic equations of motion is

$$[M]\{\ddot{q}\} + [G]\{\dot{q}\} + [K]\{q\} = \{Z\} \quad (3)$$

where  $[M]$ ,  $[G]$ , and  $[K]$  are modal mass, damping, and stiffness matrices, respectively.  $\{Z\}$  is the modal aerodynamic force vector.

With the above modal equations of motion, flutter boundaries can be computed by using coupled and uncoupled approaches.<sup>10</sup> Coupled approaches require direct time integration of flow and structural equations. Although this approach is accurate for flows with high non-linearities, it is computationally expensive. On the other hand, the uncoupled approach which is computationally less expensive requires an additional assumption that the aerodynamic data can be linearly superimposed among modes. As demonstrated in Refs. 10 and 11 earlier, and more recently in Ref. 12, the uncoupled method can be an effective approach to predict the preliminary flutter characteristics required in the early stages of design. Based on the flutter computations of airfoils in Ref. 10, the uncoupled approach requires one-tenth of the computational effort required for the coupled analysis. In this work, the uncoupled approach is used to compute the flutter boundary.

The uncoupled approach assumes that the wing will be undergoing simple harmonic motion so that the generalized coordinates  $\{q\}$  take the form

$$\{q\} = \{\bar{q}\}e^{i\omega t} \quad (4)$$

where  $\omega$  is the frequency of oscillation at flutter. Substituting Eq. (3) in Eq. (2) and introducing the concept of artificial damping,<sup>13</sup> Eq. (2) can be represented as a complex eigenvalue equation given by

$$[K]^{-1}[[M] - C[Q]]\{\bar{q}\} = \lambda\{\bar{q}\} \quad (5)$$

where generalized modal force

$$Q_{ij} = \frac{1}{S} \iint \Delta C_{pj} h_i dx dy$$

i and j represent modes.

$C = \frac{2\rho b^2 S}{k^2}$ , where  $k = \omega c/U$ , U being the flight speed.

h = modal displacement.

S = surface area of the wing.

$\lambda = \frac{(1+ig)}{\omega^2}$ , complex eigenvalue.

In this work, the standard U-g method<sup>13</sup> is used to compute the flutter boundary. In the U-g method, modal aerodynamic force matrix  $[Q]$  is required as a function of frequency for each selected mode. One way to generate the data for non-linear flows is to compute

unsteady aerodynamic data at a set of pre-selected frequencies and then interpolating the data for required frequencies in the U-g method. Typically data at 3 to 4 frequencies are required to make a reasonable prediction of the flutter boundary. The computation of data has to be repeated for all selected modes. Repeating computations for each frequency can be avoided by using the indicial approach.<sup>14</sup> In this approach, data for all frequencies can be extracted from a single unsteady response computation. The indicial approach requires an assumption that the unsteady flow can be linearized about a non-linear steady flow. Such an assumption is valid for small perturbation. It is noted that classical flutter starts as a small perturbation phenomenon and, therefore, it is appropriate to use the indicial approach to make preliminary prediction of the flutter boundary. In this work, the unsteady data required for the U-g approach is computed using the indicial approach.

## Results

### Steady Flow Computations on LANN Wing Model

To demonstrate the need of using the Navier-Stokes equations for supercritical wings, steady computations are made for the LANN supercritical wing model. It is noted that an earlier study to compute flows over this model has been performed<sup>15</sup> and showed that the inviscid potential equations are not entirely adequate to resolve the details of the flow. Furthermore, results given in this section will show that the Euler equation also do not provide adequate prediction.

The LANN model has an aspect ratio of 7.92, a taper ratio of 0.40 and a leading-edge sweep angle of 27.5 deg. The airfoil sections are supercritical with a constant thickness-to-chord ratio of 12 percent. This model was tested in the transonic wind tunnel (HST) of the National Aerospace Laboratory (NLR), the Netherlands. Details of steady flow measurements are given in Ref. 6.

Computations are made using the built-in C-H grid topology available in the wing version of ENSAERO. A grid refinement study is conducted to select a grid. The default grid of size 151x35x35 (151 points in streamwise direction, 35 points in spanwise direction and 35 points in surface-normal direction) most commonly used in ENSAERO for wing calculations and a finer grid of size 191x35x35 are selected. For both grids there are 24 spanwise sections on the wing surface. The finer grid has 960 more grid points on the wing surface than the default grid. Steady flow computations are made at  $M = 0.87$  and  $3.0$  deg AoA. The surface pressures from the default grid agrees well with those from the fine grid for all sections. Results are illustrated for 47.5% semispan section in Fig. 1. From Fig. 1 it is concluded that the 151x35x35 grid is adequate for the rest of the

calculations.

Results for  $M = 0.87$  and  $AoA = 3.0$  deg is compared with the wind tunnel measurements. Figure 2 compares the computed and measured pressures for the 47.5 percent semispan section. There are minor differences near 50% chord which are within the error limits of both the experiment and the computation. Comparisons are also good at all other sections. Euler computations were made to study the effect of viscosity for this case. Results from the Euler equations are compared with those from the Navier-Stokes equations in Fig. 3. The Euler equations give a stronger shock-wave that is located further downstream than the actual shock-wave. This result demonstrates that it is important to account for the viscous effects by using the Navier-Stokes equations for supercritical wings, even at moderate flow conditions.

One of the objectives of this work is to compare flow and aeroelastic characteristics of supercritical wings with equivalent conventional wings. This paper considers a conventional wing with NACA64A012 airfoil sections that has the same planform and thickness ratio as the LANN wing. Figure 4 shows the comparison of steady pressures between LANN and conventional wings for the 47.5 percent semispan. As expected, the supercritical wing has higher lift than the conventional wing. The additional lift comes from lower negative pressures on the upper surface and higher positive pressures near the trailing edge lower surface due to aft-loading. The LANN wing gives about 30 percent more total lift than the conventional wing. Upper surface pressure contours and simulated oil flow patterns are given for both wings in Fig. 5. Figures 4 and 5 illustrate a stronger transonic shock wave located further downstream for the LANN (supercritical) wing. Effects of these and other aerodynamic characteristics on the flutter boundary will be illustrated in the following section.

### Aeroelastic Computation on LANN Wing Model

One of the main purposes of this work is to study the aeroelastic characteristics of advanced transonic wings. For this purpose, the LANN wing is modeled as a uniform plate of thickness 0.1 inch with a root chord length of 14.2 inches which is the same as the wind tunnel rigid model. The first bending( $\omega_{h1}$ ), first torsion( $\omega_{a1}$ ), second bending( $\omega_{h2}$ ) and second torsional( $\omega_{a2}$ ) frequencies of this model are 2.98, 15.68, 37.0 and 48.68 Hz, respectively. These frequencies represent structural properties of a typical transport wing. Computations are made for Mach numbers ranging from 0.60 to 0.85 in increments of 0.025 at an AoA

of 3.0 deg.

As stated earlier the flutter boundaries are computed using the U-g method with the required unsteady data generated from the indicial method. In this work, indicial responses of sectional lifts and moments are computed for the rigid wing by giving a step change in the AoA. These indicial responses are used to compute the generalized modal forces required for the U-g approach. The validity of using the indicial approach is verified by computing the unsteady aerodynamic data both by time-integration and the indicial approach at  $M = 0.80$  and  $AoA = 3.0$  deg.

For time integration, the unsteady data is obtained by integrating the aerodynamic equations when the wing is oscillating in pitch motion about an axis located at the 50% root chord. Indicial responses are obtained by giving a step change in pitching AoA of 0.1 deg. Figure 6 shows the magnitude of sectional lifts computed from both methods for a reduced frequency  $k = 0.30$ . About 5000 time steps are required for the indicial response to reach a steady state condition with a computational time step size of 0.00325. The total CPU time required for the indicial response including the time required for the steady-state initial solution is about 2.5 hours on a single Cray C-90 processor. This is based on the fact that ENSAERO runs at about 400 MFLOPS and requires about 7 micro sec per time step per grid point. The time-integration method required three cycles with 3600 time steps per cycle (the computational step size is equal to 0.00725) for a complete calculation. This computation required about 4.5 CPU hours. Figure 6 shows that throughout the span, the indicial lift is about 2% less than the time-integration lift. This result shows a good agreement between the methods. The corresponding phase angles are plotted in Fig. 7 which also shows a good agreement throughout the wing span. These results demonstrate that the indicial approach is adequate to compute the unsteady aerodynamic data.

Since the indicial data is computed on a rigid wing, an additional assumption that the sectional forces depend mainly on the local sectional displacements is required to extend the indicial data to flexible modes. Again this assumption is valid for small perturbations. This is validated by comparing the unsteady data computed by the indicial approach on a rigid wing with that computed by time integration on a flexible wing. Both wings were oscillated in their first torsional modes at  $M = 0.80$  and  $AoA = 0.0$  deg. Figure 8 compares the magnitude of sectional lifts between indicial and time-integration methods. The lift values for each section are scaled with respect to the tip AoA of 1 deg. Both curves show the same trend. Inboard of 40% semispan, the indicial approach predicts higher lift than the that

from the time-integration approach. Outboard of 40% semispan the trend is opposite. Phase angles compare favorably between the two methods.

Steady-state solutions are computed for Mach numbers from 0.60 to 0.85 in increments of 0.025 which are required as starting solutions for computing the indicial responses. Figure 9 shows the plots of upper surface pressures at 50% semispan station for the LANN wing. The shockwave starts developing at about  $M = 0.75$  and grows stronger with an increase in Mach number. As  $M$  reaches 0.85 the flow starts separating behind the shockwave. Figure 10 shows similar plots for the conventional wing. For this case, the shockwave starts developing at  $M = 0.80$ . The influence of Mach number on total lift is shown for both wings in Fig. 11. Rate of increase in the lift starts falling for the conventional wing at  $M = 0.825$ , slightly before it occurs for the LANN wing at about  $M = 0.84$ . The effects of Mach number on center of pressures (CP) are shown in Figs. 12 and 13 for the LANN and conventional wings, respectively. For the LANN wing, inboard of 40% semispan the CP line is behind the elastic axis located at the 50% chord. Outboard of 40% semispan the CP line is in front of the elastic axis. For the conventional wing, most of the CP line is located behind the wing elastic axis except near the tip section. For both wings, the CP line moves aft with increasing Mach number. For the LANN wing the location of the CP line is slightly less sensitive to Mach number than that for the conventional wing.

Indicial responses are computed for all Mach numbers starting from the converged steady state solutions. Flutter speeds are computed by using the U-g method based on the unsteady aerodynamic data obtained from the indicial method. Fig. 14 shows a plot of flutter speed  $\bar{U}$  ( $= 2U/c\omega_{\alpha 1}$  where  $U$  is the flutter speed) versus Mach number for both wings. Flutter speeds are lower for the LANN wing than for the conventional wing. For the LANN wing the 'transonic dip' occurs at about  $M = 0.775$ . In Ref. 16 an analysis was made to relate the flutter boundary behavior to the basic flow characteristics. Based on two-dimensional airfoil calculations in Ref. 16 it is observed that the flutter speed decreases with increase in lift. Similar behavior is also observed by comparing Fig. 14 and Fig. 11. In Ref. 16 it was also observed that the flutter speed increases as the CP line moves towards the elastic axis. Since a part of the CP line inboard of 40% semispan moves towards elastic axis, and the rest moves away from the elastic axis there is more influence of lift than CP line on the flutter curve for the LANN wing. As a result there is sharper drop in the flutter speed. However, as the lift starts leveling off near peak lift, the flutter speed starts increasing. Similar behavior is also observed for

the conventional wing. However, this wing has a less sharper dip since most of the CP line moves towards the elastic axis. Therefore there is a continuous compensating effect of lift and CP line location on the flutter curve. The dip which occurs near  $M = 0.775$  is less severe than that for the LANN wing. These observations agree with those made in Ref. 2 based on wind-tunnel measurements.

### Steady Flow Computations on Wing-Body Model

The Boeing 7J7 configuration is designed to cruise at transonic Mach numbers and has been extensively wind-tunnel tested at NASA Ames Research Center. Steady flow computations were made for several flow conditions by using an H-O type grid of size  $128 \times 91 \times 38$ . The comparison of computed surface steady pressures with the experiment at 70% is shown in Fig. 15 for  $M = 0.80$ ,  $AoA = 4.0$  deg and  $Re = 8.6$  million. The comparisons are favorable.

In the earlier section, it was shown that the wing flutter boundary is dependent upon variation of lifts and center of pressures (CP) with Mach number. It is of interest to make a similar study for the wing-body configuration. Steady pressures are computed for Mach numbers ranging from 0.70 to 0.90 in increments of 0.02 at  $AoA = 4$  deg. The effect of Mach number on the total lift coefficient and CP lines are shown in Figs. 16 and 17, respectively. The CP lines are more sensitive to the increase in Mach number than the lift. The CP lines move towards the midchord with increasing Mach number. The total lift keeps increasing even after  $M = 0.90$ . From these observations and those made for the wing, it can be predicted that the flutter speed will continuously drop until  $M = 0.90$ . The transonic-dip will most likely occur at a Mach number higher than 0.90. However, a further detailed aeroelastic study, similar to that for wing, is required to confirm these observations.

### Conclusions

Detailed aerodynamic and aeroelastic computations are made for transonic wing configurations. The use of indicial response data in predicting preliminary flutter characteristics is demonstrated by using an uncoupled approach. Each flutter point required a computational time about three times that of steady-flow computations. This is considerably less, by almost a factor of 10, than the time-integration method used in the coupled approach. However, it should be noted that the present approach is valid only for small unsteady perturbations about a non-linear steady-state solution. Since flutter starts as a small perturbation phenomenon, the present approach is computationally efficient in predicting preliminary flutter characteristics.

The flutter and aerodynamic characteristics of transonic wings are compared with conventional wings. For both wings, it is found that the trend of the flutter curve is indirectly related to the flow characteristics such as lift and center of pressures. The dip in the flutter curves are successfully predicted for both wings and they are correlated with the basic flow characteristics.

Most of the current computations are limited to wing models with assumed structural properties. Further computations using realistic structural data will be made for the wing-body configurations.

### References

- <sup>1</sup> Goldhammer, M.I. and Steinle F.W., "Design and Validation of Advanced Transonic Wings Using CFD and Very High Reynolds Number Wind Tunnel Testing," ICAS 90-2.6.2, 17th Congress, Stockholm, Sweden, September 9-14, 1990.
- <sup>2</sup> Farmer, M.G., Hanson, P.W. and Wynne, E.C., "Comparison of Supercritical and Conventional Flutter Characteristics," NASA TM X-72837, May 1976.
- <sup>3</sup> Guruswamy, G.P. "Vortical Flow Computations on a Flexible Blended Wing-Body Configuration," AIAA Journal, Vol. 30, No. 10, October 1992, pp 2497-2503.
- <sup>4</sup> Guruswamy, G.P. and Byun, C., "Fluid-Structural Interactions Using Navier-Stokes Flow Equations Coupled with Finite Element Structures," AIAA-93-3087, 24th Fluid Dynamics Conference, Orlando FL, July 6-9, 1993.
- <sup>5</sup> Guruswamy, G.P., "ENSAERO - A Multidisciplinary Program for Fluid/Structural Interaction Studies of Aerospace Vehicles," Computing Systems Engineering, Vol. 1, Nos. 2-4, 1990, pp237-256.
- <sup>6</sup> Horsten, J.J., den Boer, R.G., and Zwaan, "Unsteady Transonic Pressure Measurements on a Semispan Wind Tunnel Model of A Transport-Type Supercritical Wing, Part I General Description, Aerodynamic Coefficients and Vibration Modes," AFWAL-TR-83-3039, Air Force Wright Aeronautical Laboratories, April 1982.
- <sup>7</sup> Peyret, R. and Viviani, H., "Computation of Viscous Compressible Flows Based on Navier-Stokes Equations," AGARD AG-212, 1975.
- <sup>8</sup> Beam, R. and Warming, R.F., "An Implicit Finite-Difference Algorithm for Hyperbolic Systems in Conservation Law Form." J. of Comp. Phys., Vol. 22, No. 9, Sept. 1976, pp. 87-110.
- <sup>9</sup> Obayashi, S., Guruswamy, G.P., and Goorjian,

- P.M., "Streamwise Upwind Algorithm for Computing Unsteady Transonic Flows Past Oscillating Wings," AIAA Journal, Vol. 29, No. 10, Oct. 1991, pp 1668-1677.
- 10 Guruswamy, P. and Yang, T.Y., "Aeroelastic Time Response Analysis of Thin Airfoils by Transonic Code LTRAN2," Computers and Fluids, Vol. 9, No. 4, Dec. 1980, pp. 409-425.
  - 11 Guruswamy, P. and Goorjian, P.M., "Computations And Aeroelastic Applications of Unsteady Transonic Aerodynamics About Wings," JI of Aircraft, Vol. 21, NO. 1, Jan 1984, pp 37-43.
  - 12 Lee-Rausch, E. L. and Batina, J. T, "Calculation of AGARD wing 445.6 Flutter Using Navier-Stokes Aerodynamics," AIAA Paper No. 93-3476, AIAA 11th Applied Aerodynamics Conf. Aug 1993.
  - 13 Fung, Y.C. , "Section 6.11, An Introduction To The Theory of Aeroelasticity," Dover Publications, Inc, New York 1965,
  - 14 Ballhaus, W.F. and Goorjian, P.M. , "Computation of Unsteady Transonic Flow by Indicial Method," AIAA J, NO 2, Vol 16, Feb 1978, pp 117-124.
  - 15 Malone, J.B and Ruoo, S.Y., "LANN Wing Test Program: Acquisition and Application of Unsteady Transonic Data for Evaluation of Three-Dimensional Computational Methods," AFWAL-TR-83-3006, Air Force Wright Aeronautical Laboratories, Feb 1983.
  - 16 Yang, T.Y., Guruswamy, G. P., Striz, A.G. and Olsen, J.J., "Reply by Authors to H.P.Y. Hitch," JI. of Aircraft, Vol. 18, No. 2, February 1981, pp. 159-160.

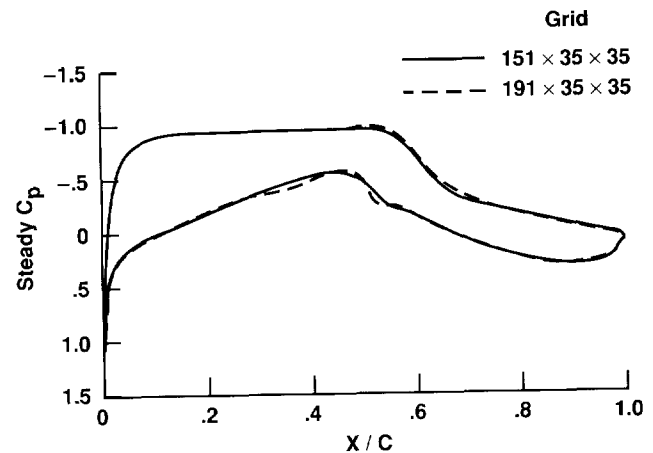


Fig. 1 Effect of grid refinement on pressure distribution at  $M = 0.87$  and  $\alpha = 3$  deg for 47.5% section.

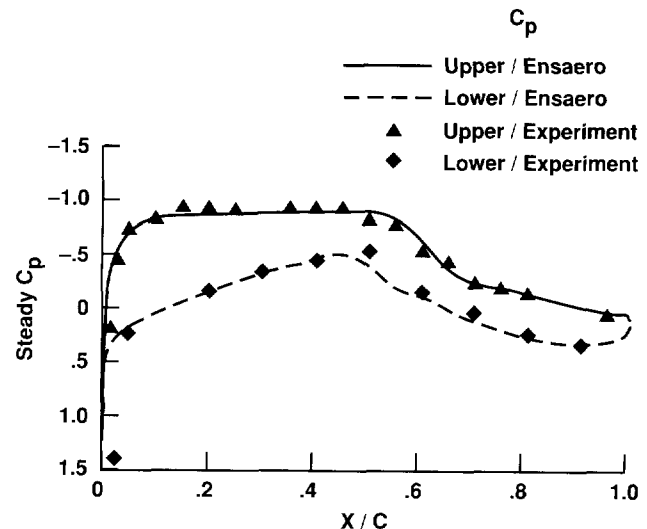


Fig. 2 Comparison between computed and measured pressure distributions at  $M = 0.87$  and  $\alpha = 3$  deg for 47.5% section.

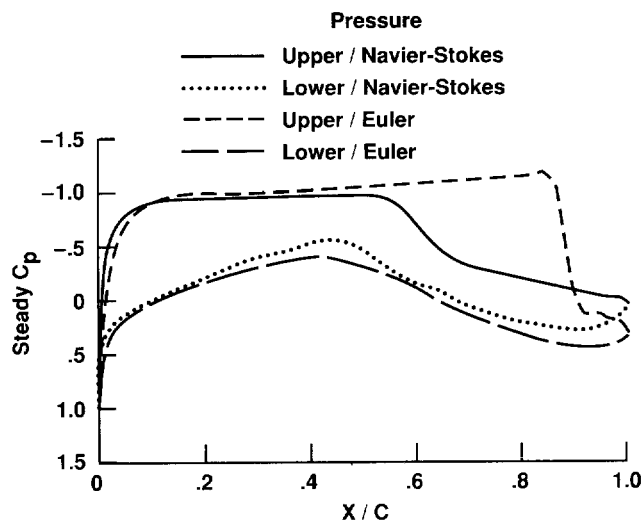


Fig. 3 Comparison of between pressure distributions from the Euler and Navier-Stokes equations at  $M = 0.87$  and  $\alpha = 3$  deg for 47.5% section.

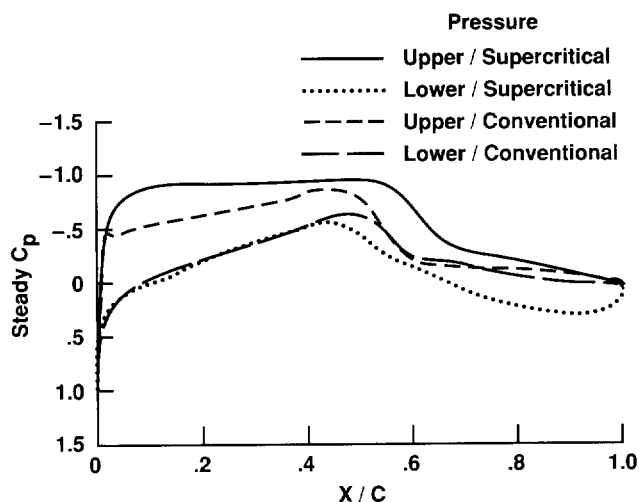
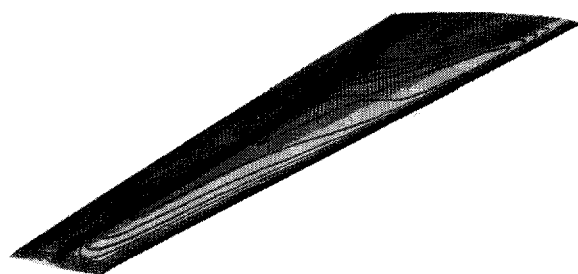
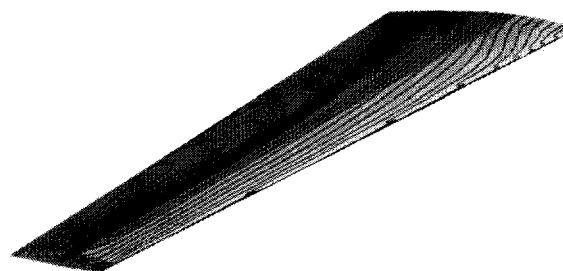


Fig. 4 Comparison between pressure distributions for supercritical and conventional wings at  $M = 0.87$  and  $\alpha = 3$  deg for 47.5% section.

### Surface Pressure Contours

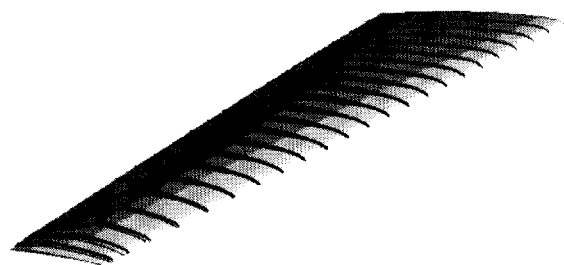


Supercritical Wing

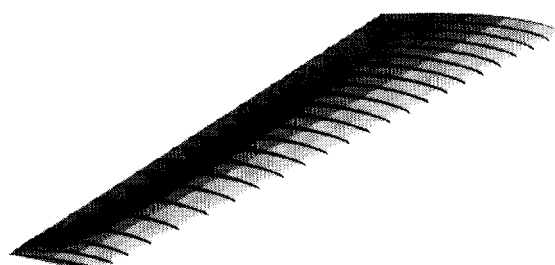


Conventional Wing

### Simulated Oil Flow



Supercritical Wing



Conventional Wing

Fig. 5 Comparison of surface flow characteristics between supercritical and conventional wings at  $M = 0.87$  and  $\alpha = 3$  deg.

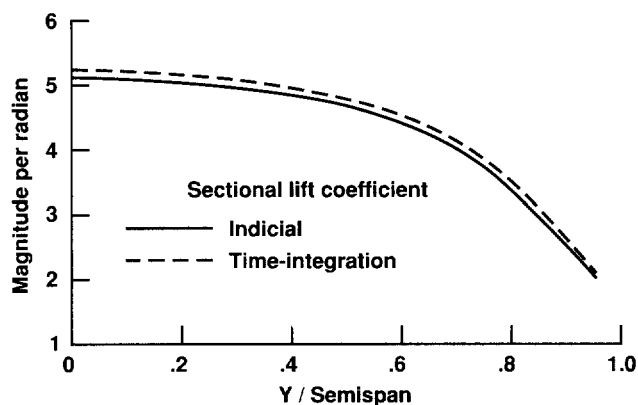


Fig. 6 Comparison of magnitude of sectional lifts between indicial and time integration method for  $M = 0.80$ ,  $\alpha = 3$  deg and  $k = 0.30$ .

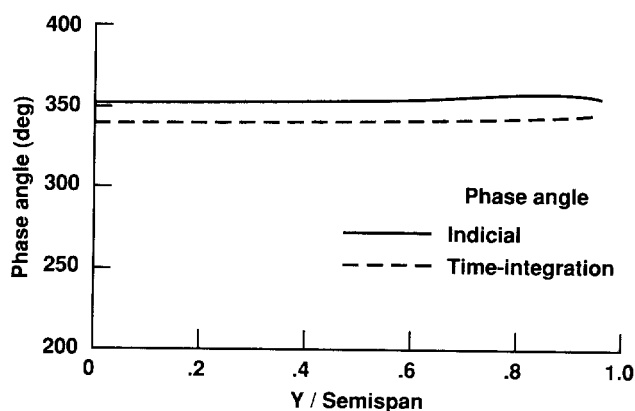


Fig. 7 Comparison of phase angles of sectional lifts between indicial and time integration method for  $M = 0.80$ ,  $\alpha = 3$  deg and  $k = 0.30$ .

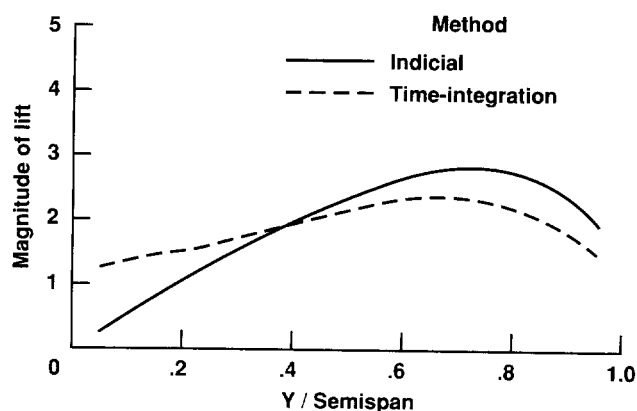


Fig. 8 Comparison of magnitude of sectional lifts between indicial method for rigid wing and time integration method for flexible wing at  $M = 0.80$ ,  $\alpha = 3$  deg and  $k = 0.30$ .

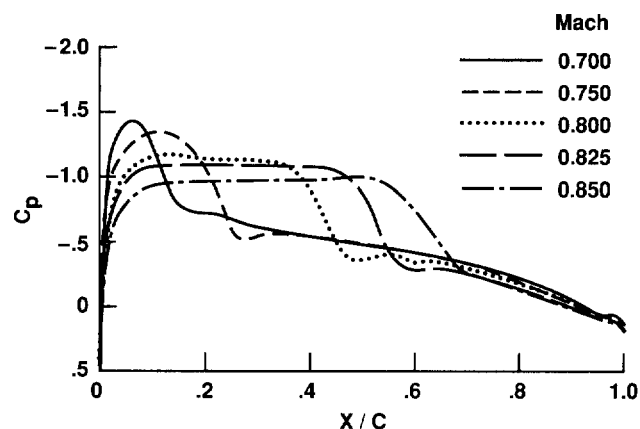


Fig. 9 Effect of Mach number on pressure distributions at 47.5% section for supercritical wing at  $\alpha = 3$  deg.

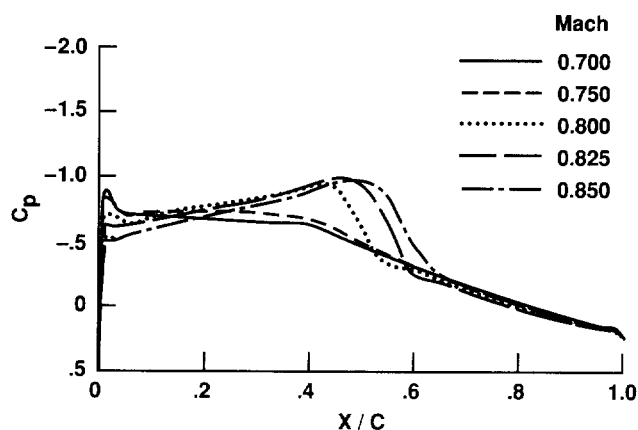


Fig. 10 Effect of Mach number on pressure distributions at 47.5% section for conventional wing at  $\alpha = 3$  deg.

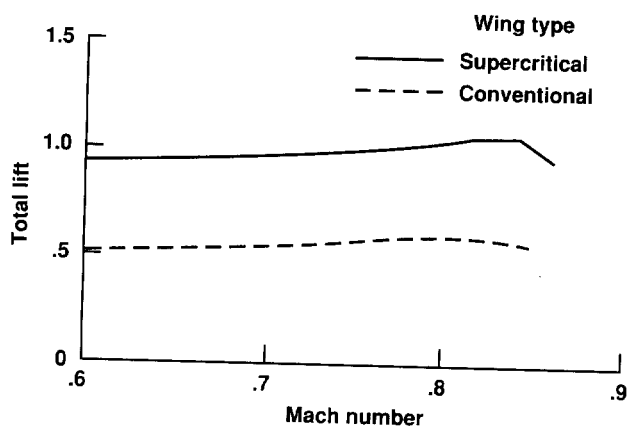


Fig. 11 Comparison of total lift vs Mach number plots between supercritical and conventional wings for  $\alpha = 3$  deg.



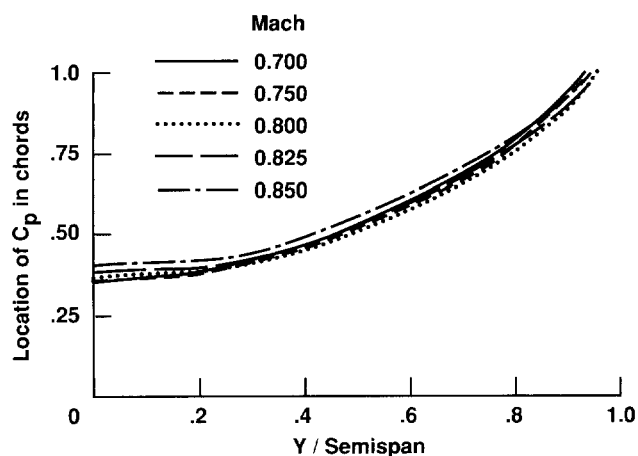


Fig. 12 Effect of Mach number on center of pressure distributions for supercritical wing at  $\alpha = 3$  deg.

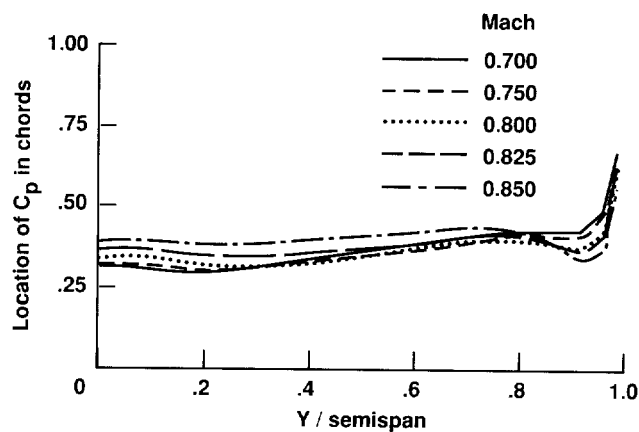


Fig. 13 Effect of Mach number on center of pressure distributions for conventional wing at  $\alpha = 3$  deg.

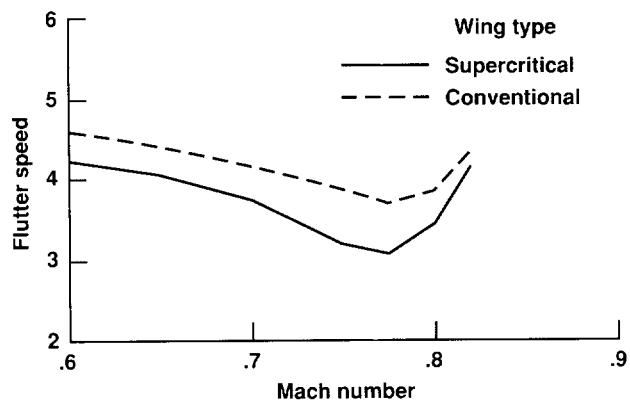


Fig. 14 Comparison of flutter boundaries between supercritical and conventional wings at  $\alpha = 3$  deg.

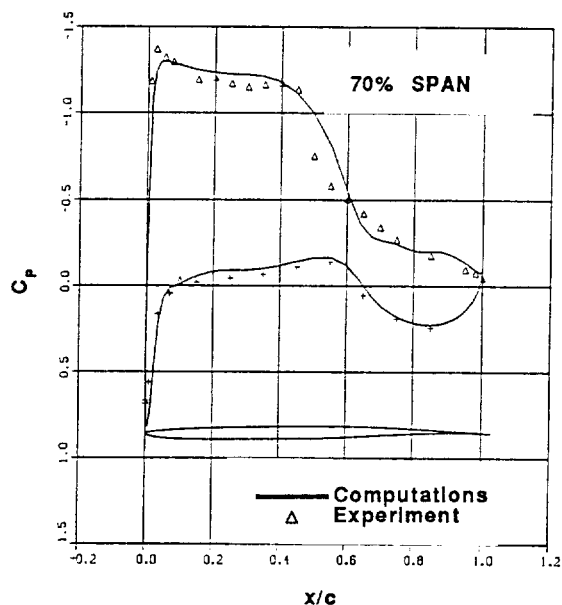


Fig. 15 Comparison of computed surface pressures with experiment for the wing-body configuration at  $M = 0.80$  and  $\alpha = 4$  deg.

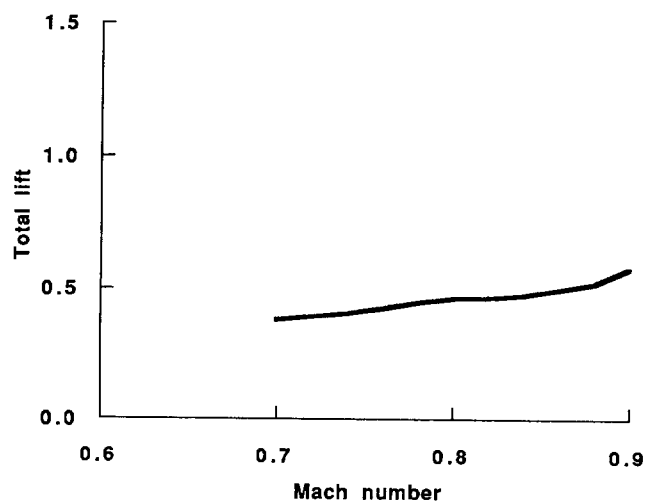


Fig. 16 Effect of Mach number on total lift for wing-body configuration at  $\alpha = 4$  deg.

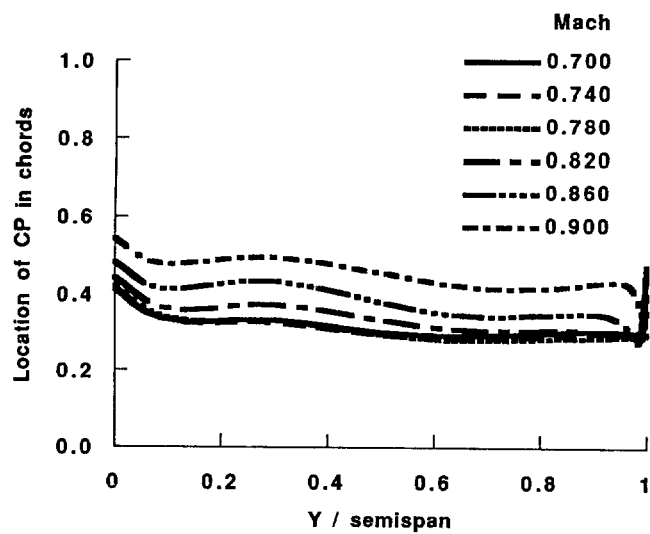


Fig. 17 Effect of Mach number on center of pressure lines for wing-body configuration at  $\alpha = 4^\circ$ .